Journal of
Composites Science

MDPI

Article

Development and Evaluation of 3D-Printed PLA/PHA/PHB/HA Composite Scaffolds for Enhanced Tissue-Engineering Applications

Motahareh Sadat Raziyan [1,*], Arvydas Palevicius [1,*], Dariusz Perkowski [2], Sigita Urbaite [1] and Giedrius Janusas [1]

[1] Faculty of Mechanical Engineering and Design, Kaunas University of Technology, Studentu st. 56, 51424 Kaunas, Lithuania; sigita.urbaite@ktu.lt (S.U.)
[2] Faculty of Mechanical Engineering, Bialystok University of Technology, Wiejska 45A, 15-351 Biaystok, Poland; d.perkowski@pb.edu.pl
* Correspondence: motahareh.raziyan@ktu.edu (M.S.R.); arvydas.palevicius@ktu.lt (A.P.)

Abstract: Recently, tissue engineering has been revolutionised by the development of 3D-printed scaffolds, which allow one to construct a precise architecture with tailored properties. In this study, three different composite materials were synthesised using a combination of polylactic acid (PLA), polyhydroxyalkanoates (PHA), poly(3-hydroxybutyrate) (PHB) and hydroxyapatite (HA) in varying weight percentages. Morphological properties were evaluated by scanning electron microscopy showing a uniform distribution of HA particles throughout the matrix, indicating good compatibility between the materials. Furthermore, the printed scaffolds were tested under pressure using a load cell to examine mechanical strength. Scanning electron microscopy (SEM) analysis showed favorable dispersion, biological compatibility together with enhanced bioactivity within the PHB/PHA/PLA/HA composite matrixes. Thus, this paper demonstrates the successful design and implementation of these composite structures for tissue-engineering applications and highlights the effective development of biocompatible scaffold designs with improved functionality.

Keywords: bone graft; tissue engineering; polymeric composite; 3D printing

Citation: Raziyan, M.S.; Palevicius, A.; Perkowski, D.; Urbaite, S.; Janusas, G. Development and Evaluation of 3D-Printed PLA/PHA/PHB/HA Composite Scaffolds for Enhanced Tissue-Engineering Applications. *J. Compos. Sci.* **2024**, *8*, 226. https://doi.org/10.3390/jcs8060226

Academic Editor: Francesco Tornabene

Received: 23 April 2024
Revised: 5 June 2024
Accepted: 12 June 2024
Published: 16 June 2024

1. Introduction

Three-dimensional printing (3DP) has emerged as an essential approach for generating scaffolds capable of replacing autografts and allografts. Tissue engineering has become an intriguing topic for the development of biological alternatives for the repair or replacement of damaged tissues or organs [1]. However, there is still a shortage of manufacturing procedures that can replicate both the mechanical and biological capabilities of native bones [2]. Three-dimensional bioprinting is a significant advancement in tissue engineering, allowing research on novel biomaterials and potentially offering applications in tissue regeneration in surgical and prosthetic applications [3]. Today, great attention is paid to developing printable materials (inks) that are mechanically strong, biocompatible and degradable and support tissue regeneration. Organ printing is a novel approach to cell-based tissue engineering allowing to create cell-laden hydrogel scaffolds with a tailored external shape and internal morphology [4].

Fused deposition modelling (FDM) is one of the possible manufacturing technologies for these applications due to its simplicity, the ability to produce complex parts and adjustable shapes, and its low operating costs [5]. FDM can be used to create composite scaffolds with highly controlled material distribution and pore architecture. Usually, the natural healing process of bones is slow, and a bone grafting procedure is required to improve the patient's condition quickly. Therefore, bone grafting procedures such as autographs, allographs and xenografts have limitations and bone replacement is created through additive manufacturing using biomaterials in the form of a bone scaffold [6]. Polymeric scaffolds, which act as a physical support for regenerating tissue, are frequently

used in bone tissue regeneration. Polymer-based materials have developed intriguing possibilities for bone tissue formation due to their distinct properties and wide range of applications [7,8]. Therefore, due to low variation between batches, biodegradable natural polymers have a wide range of medical applications. As, for example, polylactic acid (PLA) and its copolymers became widely used in tissue engineering for function restoration of impaired tissues, because of their excellent biocompatibility and mechanical properties. PLA scaffolds provide an ideal environment for cell adhesion, proliferation and differentiation [9]. Several PLA blends have been investigated for use in biomedical applications such as drug delivery, implants, sutures and tissue engineering [10].

For porous bone repair scaffold fabrication, researchers combined PLLA (L-polylactic acid)/nano-hydroxyapatite (nHA) composite with low-cost fused deposition modelling (FDM) technology. The results showed that the designed PLLA/nHA composite ink met the printing smoothness and accuracy requirements for personalised bone-repair applications. However, it was noticed that synthetic biodegradable polymers lacked differentiation properties compared to natural biodegradable polymers, but gained the ability to control mechanical properties, tailorable porosity and degradation time while maintaining biocompatibility [11].

For tissue-engineering applications, polyhydroxyalkanoates (PHAs) are widely used materials belonging to the family of biodegradable and biocompatible polymers. Poly(3-hydroxybutyrate) (PHB) has attracted considerable attention among PHA due to its beneficial features, such as biocompatibility, biodegradability and processability [12], and may replace fossil-derived polymers. Polyhydroxybutyrate (PHB) is a short-chain polyhydroxyalkanoate (PHA) that is naturally produced by a variety of microorganisms as a carbon and energy reserve. PHB has high mechanical strength and can be used to create scaffolds using additive manufacturing techniques, such as three-dimensional (3D) printing. It is one of the most promising alternatives to petroleum-based plastics [13]. Biomaterials such as titanium (Ti), iron (Fe), magnesium (Mg) and zinc (Zn) have been studied over the years to fulfil requirements for increased bioactivity. During the past decade, magnesium (Mg) and related alloys received considerable attention for bone fracture repair due to their properties, such as good mechanical strength, strong biocompatibility and progressive decomposition (without the production of biotoxic byproducts). Mg-based metals can deteriorate quickly and efficiently, releasing Mg ions and making them suitable for supporting a variety of biological processes and as protective coatings for Mg-based products. Also, Mg ions are linked to different biofunctionalities, such as boosting angiogenesis, improving osteogenesis and anti-inflammatory characteristics.

Recently, it was found that the addition of bioactive materials such as hydroxyapatite (HA) may improve the osteoconductivity and bioactivity of PHB scaffolds for bone tissue engineering. The mineral HA is a key component of natural bone and has good biocompatibility and osteoinductive properties. Thus, the combination of PHB and HA has gained the potential to produce composite materials that replicate the structural and functional properties of bone. In Micaela Degli's study, fused deposition modelling (FDM) technology was used to prepare the composite scaffolds of polylactic acid (PLA) and nanohydroxyapatite (nHA). The results demonstrated that the proposed PLA/n-HA compounds were highly printable and the printed scaffold had tenable mechanical strength as a function of components of the number of n-HA [14]. The biocompatibility and osteogenic induction capabilities of the pure PLA scaffold were demonstrated to be superior. The use of polymers and ceramics as composite material for 3D printing via FDM (Fused Deposition Modelling) has been investigated, and results showed enormous potential in bone tissue engineering. The use of FDM to create PHB/PHA-HA composite scaffolds allowed the implementation of a viable technique to create patient-specific bone replacements and implants with improved osteoconductive and mechanical integrity [5]. This work is original in its synthesis and evaluation of novel 3D-printed scaffolds combining PLA, PHA, PHB and HA in varying weight percentages, demonstrating improved mechanical strength and bioactivity compared to previously cited studies.

2. Materials and Methods

Three different concentrations of composite materials were synthesised for the design of 3D-printed scaffolds. Many experiments were conducted until the best ratio between different concentrations of material and required properties was found.

2.1. Preparation of Materials

Five main materials PLA, PHA, PHB, HA and Mg were used for the synthesis of biocomposites. However, before they could be used for synthesis, the HA particles and polymer ingredients were specially prepared, as, for example, HA was available as a powder, and before use it had to be cleaned and sterilised, and the water in the HA had to be removed by centrifugation.

The results in Figure 1 implied the size of the HA particles ranges from 500 to 900 nm.

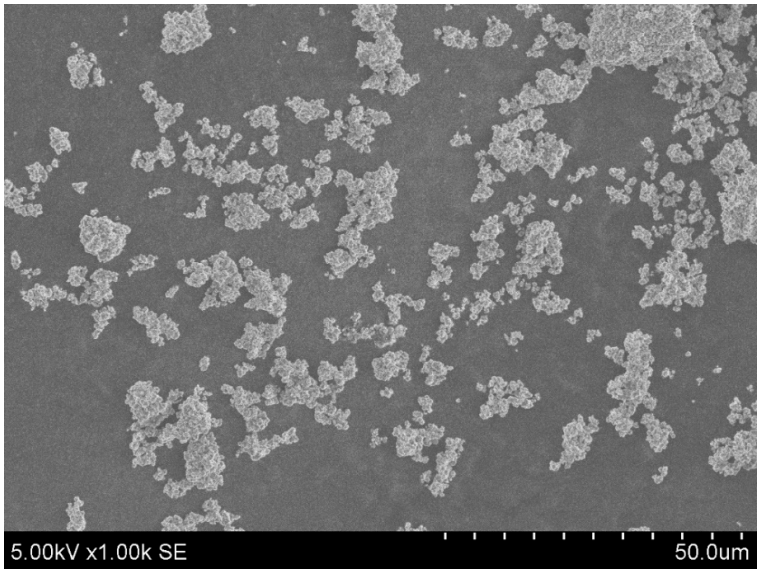

Figure 1. Image taken with a scanning electron microscope of HA powder.

2.2. Materials Synthesis

The powder hydroxyapatite was obtained from cow bones using the calcination method to synthesise, which was explained in previous work (1). Mg powder, polylactic acid (PLA), polyhydroxyalkanoates (PHA), poly(3-hydroxybutyrate) (PHB) pellet, DMSO and ACETONE were purchased from Sigma-Aldrich (St. Louis, MO, USA). A schematic of different sample preparations is given in Figure 2.

Figure 2 illustrates the comprehensive process involved in the preparation and application of PLA/HA/PHB/PHA composite scaffolds. Initially, polylactic acid (PLA), hydroxyapatite (HA), polyhydroxyalkanoates (PHA) and poly(3-hydroxybutyrate) (PHB) are synthesised, each component contributing unique properties such as osteoconductivity, biodegradability and mechanical strength. These materials are mixed to achieve a uniform distribution of HA particles within the PLA, PHB and PHA matrix. The composite material is then used in a 3D-printing process to create scaffolds with precise architectural configurations. Morphological properties and material compatibility are evaluated by SEM, while mechanical strength is assessed by load cell testing. The resulting scaffolds, designed for tissue-engineering applications, demonstrate enhanced bioactivity and functionality, supporting cell growth and tissue regeneration. This graphical representation encapsulates the innovative approach and successful implementation of these composite structures in biomedical engineering.

Figure 2. A graphical representation of the PLA/HA/PHB/PHA scaffolds' preparation.

The composite materials were prepared using polylactic acid (PLA), polyhydroxyalkanoates (PHA), poly(3-hydroxybutyrate) (PHB) and hydroxyapatite (HA). Initially, PLA, PHA and PHB polymers were mixed with HA particles in varying weight percentages to ensure uniform distribution. The mixing process was carried out using a high-shear mixer at 2000 rpm for 10 min. The resulting mixture was then extruded using a twin screw extruder at a temperature of 200 °C and a screw speed of 100 rpm to form filaments. Subsequently, these filaments were used to fabricate scaffolds using a 3D printer (XYZPrinting da Vinci 1.0 Pro), set at a nozzle temperature of 210 °C, a bed temperature of 60 °C and a layer thickness of 0.2 mm.

Due to the suitable behaviour of PLA in bone graph material, 15 wt % hydroxyapatite and 5 wt % Mg powder was used for the synthesis of biocomposites. Many experiments were conducted to find the best ratio between PLA, PHA and PHB by weight and required biocomposite properties. Thus, HA and Mg concentrations were kept the same in all three samples (see Table 1).

Table 1. Composition of fabricated samples.

Sample No.	PLA (wt %)	PHA (wt %)	PHB (wt %)	Mg (wt %)	HA (wt %)
1	30.0	30.0	20.0	5.0	15.0
2	40.0	40.0	0.0	5.0	15.0
3	60.0	0.0	20.0	5.0	15.0

Thus, the polymer pellet was dissolved in DMSO and sonicated for 3 h in a magnetic stirring machine. On the other hand, the HA and Mg powders were dissolved in acetone and sonicated for 2 h to obtain the desired suspension. The suspension was added to the polymer solution while stirring for several hours to ensure that the HA particles were evenly dispersed in the solution. Finally, the composite was obtained after the solvent volatilised for 12 h evaporation at room temperature and then was placed in an oven at 60 degrees to remove any DMSO or other solution residuals. Eventually, three different compounds were obtained, containing the same concentrations of 15% HA and 5% Mg (Table 1). Then, the resulting compounds were cut with a scissor to be used in an extrusion

to produce the desired filament (see Figure 3). Figure 3 shows the dried and scissor cut composite samples, illustrating (a) sample 1, (b) sample 2 and (c) sample 3, each prepared with different weight percentages of PLA, PHA, PHB and HA.

(**a**) (**b**) (**c**)

Figure 3. Dried and scissor cut composite samples on a 1 cm scale: (**a**) sample 1, (**b**) sample 2, (**c**) sample 3.

The main properties of the materials used for the preparation of the samples are given in Table 2, including the melting point temperature, the size of the granolite, the type of morphology and the density.

Table 2. Properties of materials for sample preparation.

	HA	PLA	PHA	PHB
Melting point temperature	1100	170–180	165–180	175–180
Granolate size	1 mm	4–6 mm	3 mm	5 mm
Morphology	spherical	spherical	cylindrical	cylindrical
Density (g/cm^3)	5.12	1.24	1.23	3.07

2.3. Filament Fabrication and Scaffold Printing

The SolidWorks software (SolidWorks 2023) was used for developing and refining objects for 3D printing, including intricate structure scaffolds. In this work, a sophisticated porous cylindrical structure, which serves as a realistic model for the scaffold under investigation, was developed. The architectural details were adjusted for precise geometric precision, to ensure the scaffold for the intended application (Figure 4).

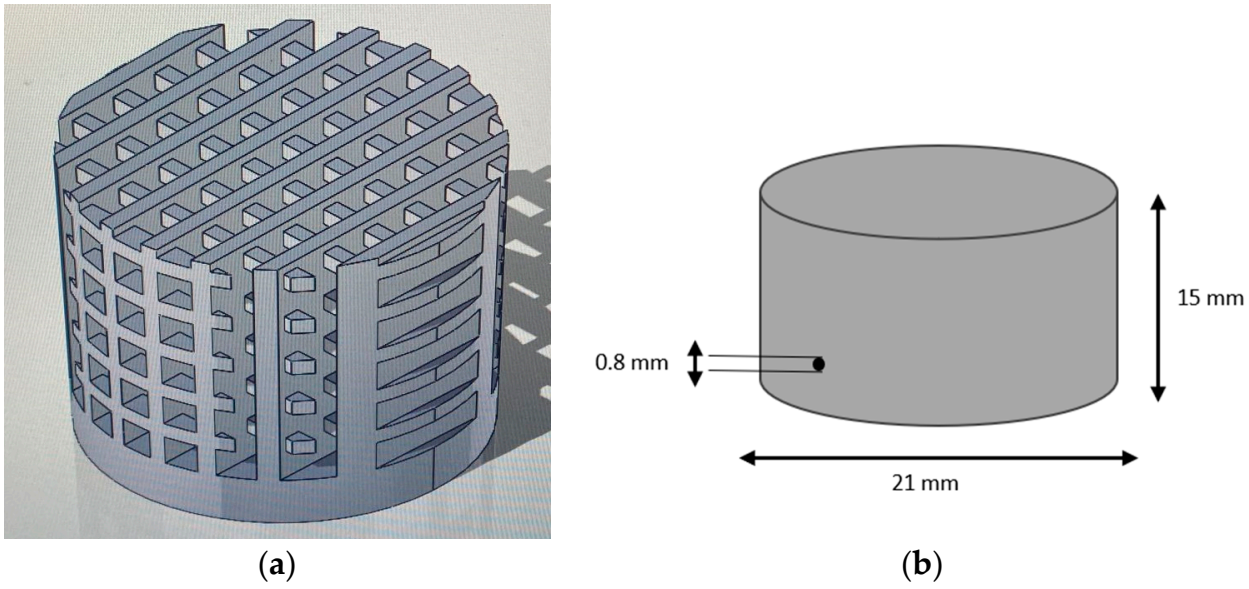

(**a**) (**b**)

Figure 4. (**a**) A 3D porous cylinder model and (**b**) the geometry.

Furthermore, for scaffold printing, the constructed composite blocks of sample 1, sample 2 and sample 3 were cut into small particles and transformed into a molten state. A twin screw extruder device (Naztek extrusion technology) was used to extrude the molten materials from different samples to produce 3D-printing filaments.

For 3D printing, a Prusa printer was used as the primary platform with a nozzle size of 0.3 mm, a layer height of 0.1 mm, and an interlayer spacing of 0.25 mm. The process was carefully arranged according to several parameters, at the same time controlling the temperature: the print bed was kept at 50 °C and the nozzle temperature was kept at 180 °C. Using a 3D printer, a complexly patterned scaffold was created by printing layer-by-layer progressive deposition of the filaments. Such printing parameters as print speed, temperature regulation and layer thickness were crucial factors in the procedure. To achieve the necessary material qualities and structural characteristics of the scaffolds, several printings were performed for optimisation of these parameters. The final result led to high-quality printed scaffold samples with a pore size of 0.8 mm (Figure 5).

(**a**) (**b**) (**c**)

Figure 5. Printed scaffold (**a**) sample 1, (**b**) sample 2, (**c**) sample 3.

2.4. Equipment Used for Investigations

Characterisation of the composite materials included several techniques. The morphology of the samples was investigated using a focused ion beam scanning electron microscope (FIB-SEM) SCIOS 2, S-3000N, located at the Bialystok University of Technology, Poland. The imaging parameters included an accelerating voltage of 10 kV, a working distance of 10 mm and magnification ranging from 100× to 10,000×.

Contact angle measurements were taken with a Krüss DSA100 geometer to evaluate surface hydrophobicity/hydrophilicity of samples. For experimentation, distilled water at room temperature was used and five measurements per sample were taken. The measurement system was located at the Faculty of Mechanical Engineering and Design, Kaunas University of Technology, Lithuania.

For characterisation of chemical composition, X-ray diffraction (XRD) was used to evaluate the crystalline structure of the composites using a PANalytical X'Pert PRO diffractometer with a Cu Kα radiation source, scanning from 10° to 80° (2θ) at a step size of 0.02° and a scan rate of 2° per minute.

Mechanical tests were carried out with an Instron 3365 dual column tabletop tensile test machine, featuring a displacement speed of 1 mm/min, a gauge length of 50 mm and a load cell capacity of 10 kN, at the same university. In addition, porosity was assessed using a Bruker SkyScan 1172 microtomography system, revealing an average pore diameter of 0.8 mm. These methods ensured a comprehensive evaluation of the mechanical and structural properties of the composite scaffolds. The measurement system was located in the Faculty of Mechanical Engineering at Bialystok University of Technology, Poland.

To measure porosity, the microtomography (Micro-CT) technique was used. It provided high-resolution, three-dimensional images of the internal structure of the samples, allowing for precise measurement of the volume of pore spaces. X-ray imaging was used to capture detailed images of the internal and external features of the samples, aiding in the visualisation and quantification of pore structures. The BRUKER SKYSCAN 1172 X-ray

microtomograph used a 100 kV 10 W lamp and an 11 Mpx CCD detector. The resolution per layer is a maximum of 4 k × 4 k pixels. The maximum resolution is 1 um. The chamber allows examination of samples with a maximum diameter of 50 mm (compound scan). Data obtained from microtomography and X-ray imaging were analysed using specialised software to calculate the volume of pore spaces and the total volume of the samples.

3. Results

The morphology, chemical structure, wettability, porosity and mechanical properties were investigated for three scaffold samples printed with a 3D printer.

3.1. Surface Morphology Investigations

Scanning electron microscopy (SEM) allowed us to perform careful analysis of the distribution and dispersion of hydroxyapatite (HA) particles within the composite matrix, made up of polylactic acid (PLA), polyhydroxyalkanoates (PHA) and poly(3-hydroxybutyrate). The SEM images were captured at varying magnifications (500, 5000, 10,000 and 15,000 times the standard electron microscope resolution) (Figure 6). Obtained results demonstrated the uniformity of HA particles and shed light on how they were arranged spatially within the matrix. The arrangement of those particles resulted in structural reliability and increased bioactivity. Moreover, obtained SEM images showed particle distribution, providing a view of how HA and the polymer matrix interact, illuminating their compatibility and potential bonding. This property is crucial because a harmonious interface is a key factor in the successful incorporation of bioactive materials within the composite scaffolds. Effective compatibility can lead to improved scaffold bioactivity and osteoconductivity and those factors are vital for tissue-engineering applications.

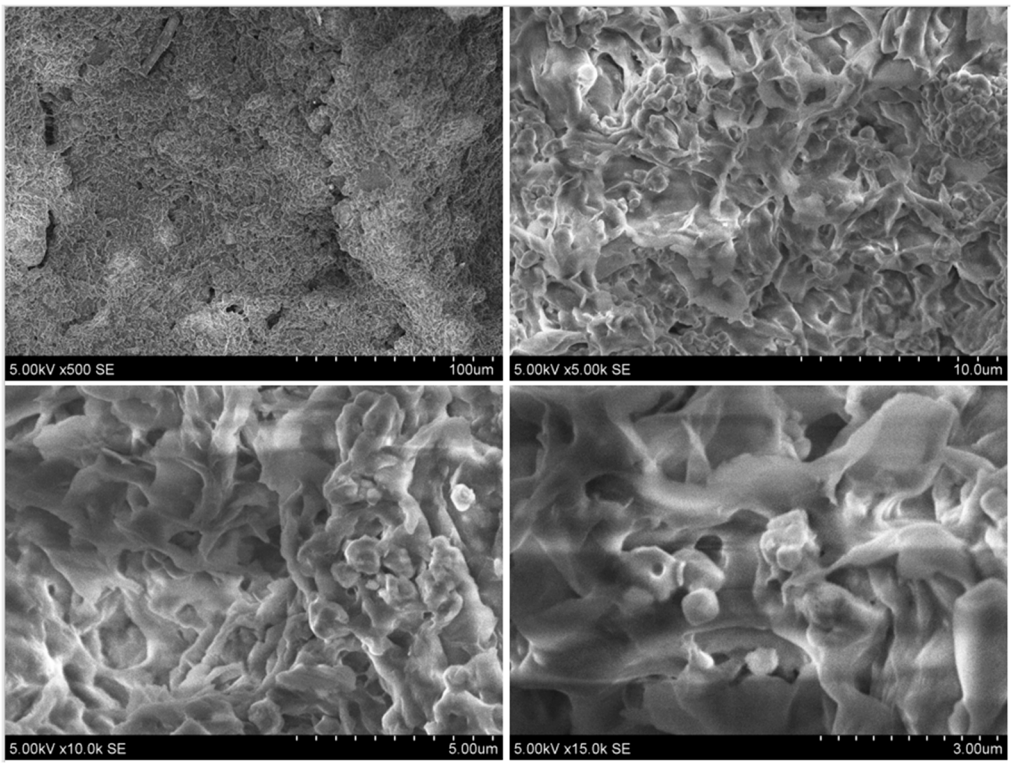

(**a**)

Figure 6. *Cont.*

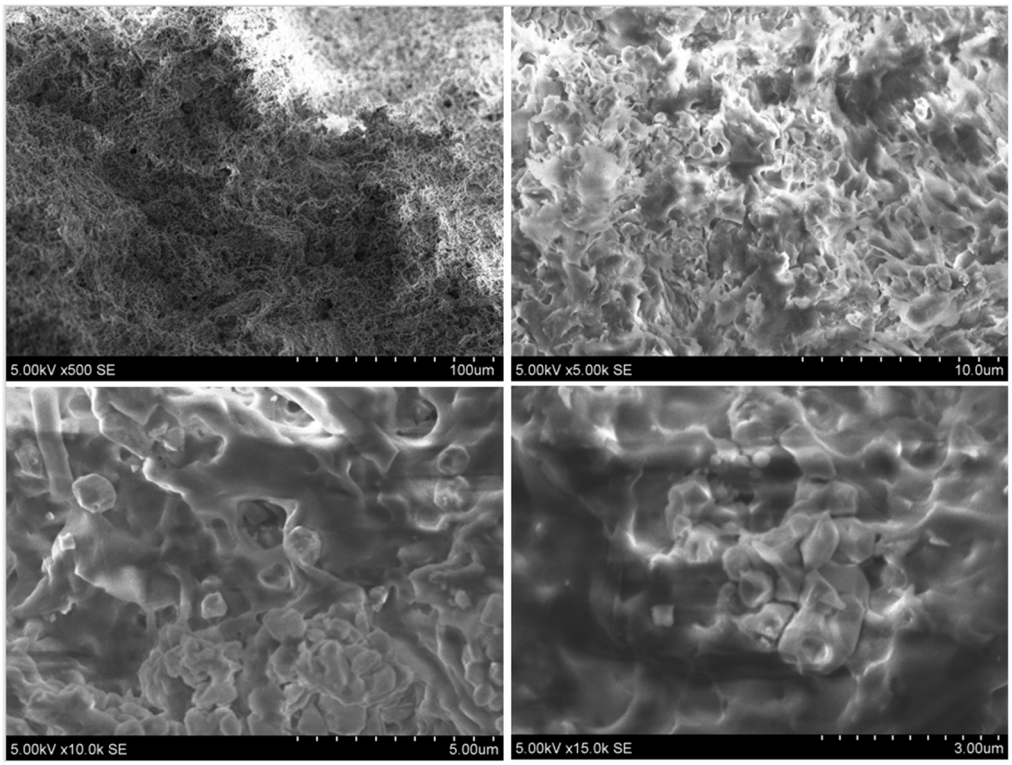

(**b**)

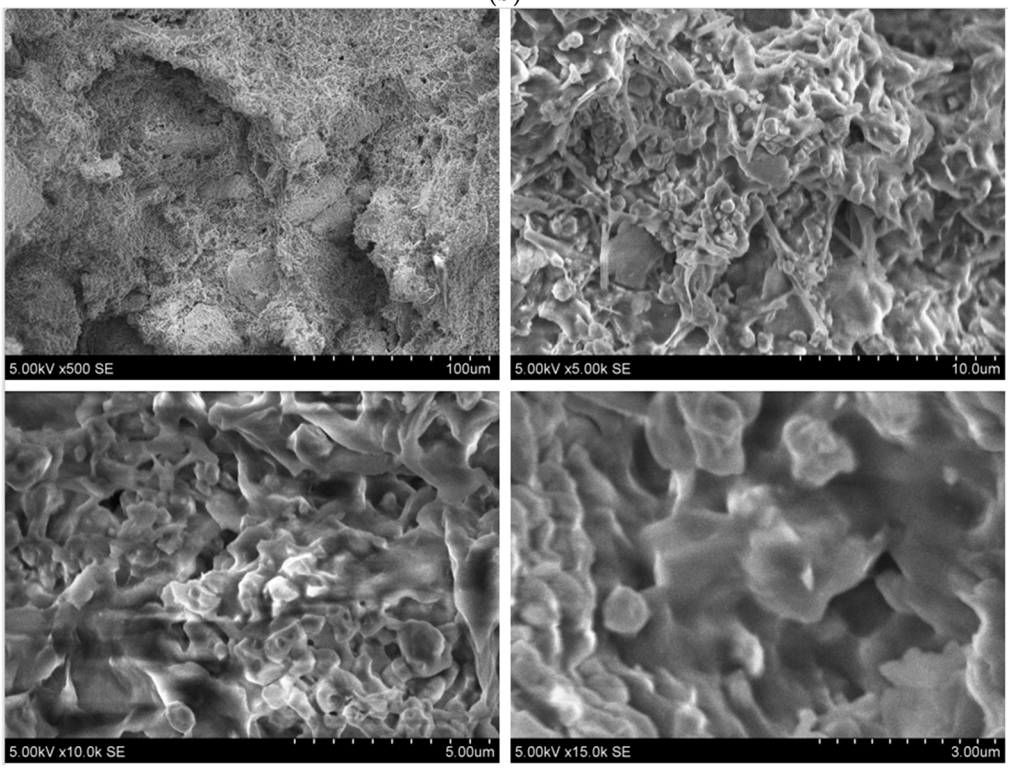

(**c**)

Figure 6. Three-dimensional images of the printed scaffold (**a**) sample 1, (**b**) sample 2 and (**c**) sample 3.

The white spheres (Figure 6a–c) are evenly distributed HA particles that were dispersed throughout the matrix. SEM images of the porous structure show the potential for increased surface area and cell infiltration, ensuring that they meet the stringent requirements of biocompatibility, mechanical stability and bioactivity required for successful

tissue regeneration. The structural characteristics of the scaffolds are crucial for their capacity to promote cell growth and facilitate tissue regeneration. As seen from 3D images (Figure 6), the designed scaffold samples show a precise porous architecture, a network, allowing it to be implemented in tissue engineering. As investigations showed, increased cell adhesion and proliferation were possible by expanding the surface area available for cellular interactions. This characteristic is especially helpful for encouraging the growth of new tissue and eventually achieving successful regeneration.

The hydrophobicity/hydrophilicity test was carried out to evaluate contact angles by placing a drop of distilled water on the clean surface of each sample. The contact angle for each 3D-printed bone transplant sample gave important information on the hydrophobicity/hydrophilicity of the surface. Contact angles were used to determine how effectively a surface repels or attracts water. Thus, obtained results showed that sample 1 with its contact angle of 37.5 degrees was hydrophilic. Sample 2 had a contact angle of 27.10 degrees, indicating a hydrophilic surface, too. Sample 3's contact angle was 56.94 degrees, indicating the surface was also hydrophilic. The water droplets were spread on the surface of samples indicating fast water attraction. The obtained results provided understanding concerning how the samples may behave when in contact with biological or other environments.

3.2. Chemical Composition

The X-ray energy dispersive spectroscopy (EDS) technique was used to determine the elemental composition of materials, allowing the individual elements present in the composites to be identified, and ensuring that the composite includes the necessary components to promote bone growth and integration. Trace elements or contaminants can sometimes affect the biocompatibility and safety of medical implants, such as bone transplants. Based on the EDS results (Figure 7), the composition of the samples indicated that each has a combination of organic and inorganic components, with a focus on elements that are important for bone health and regeneration (such as calcium, magnesium and phosphorus).

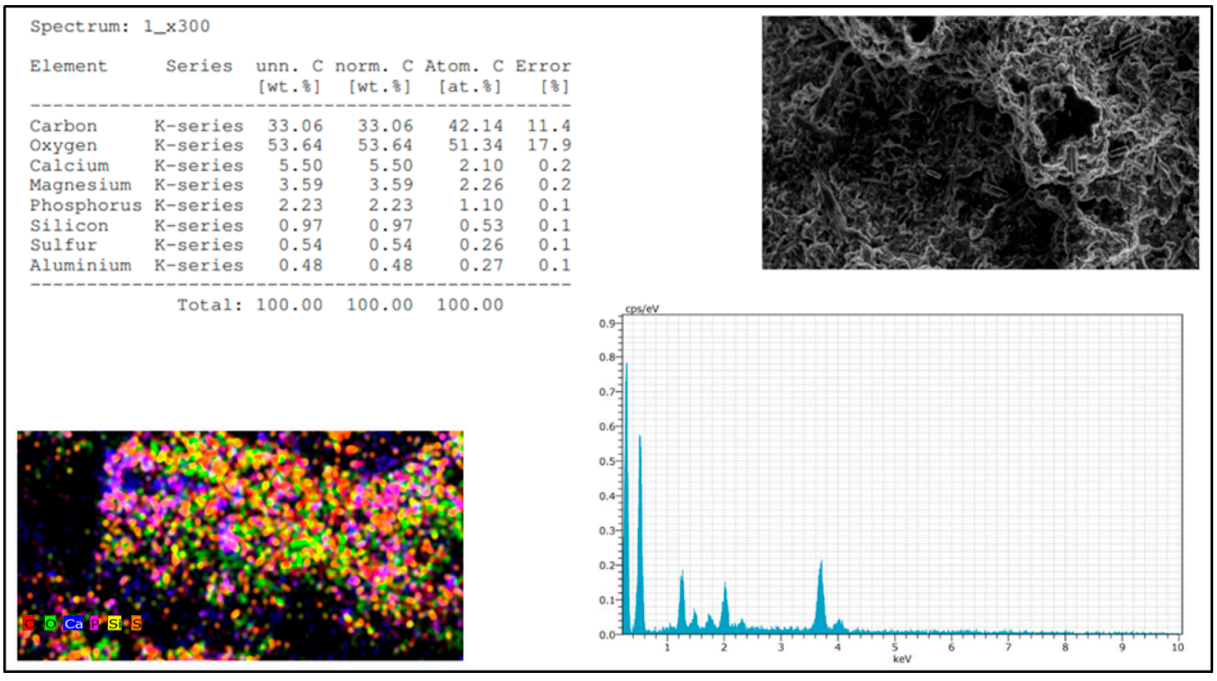

(**a**)

Figure 7. *Cont.*

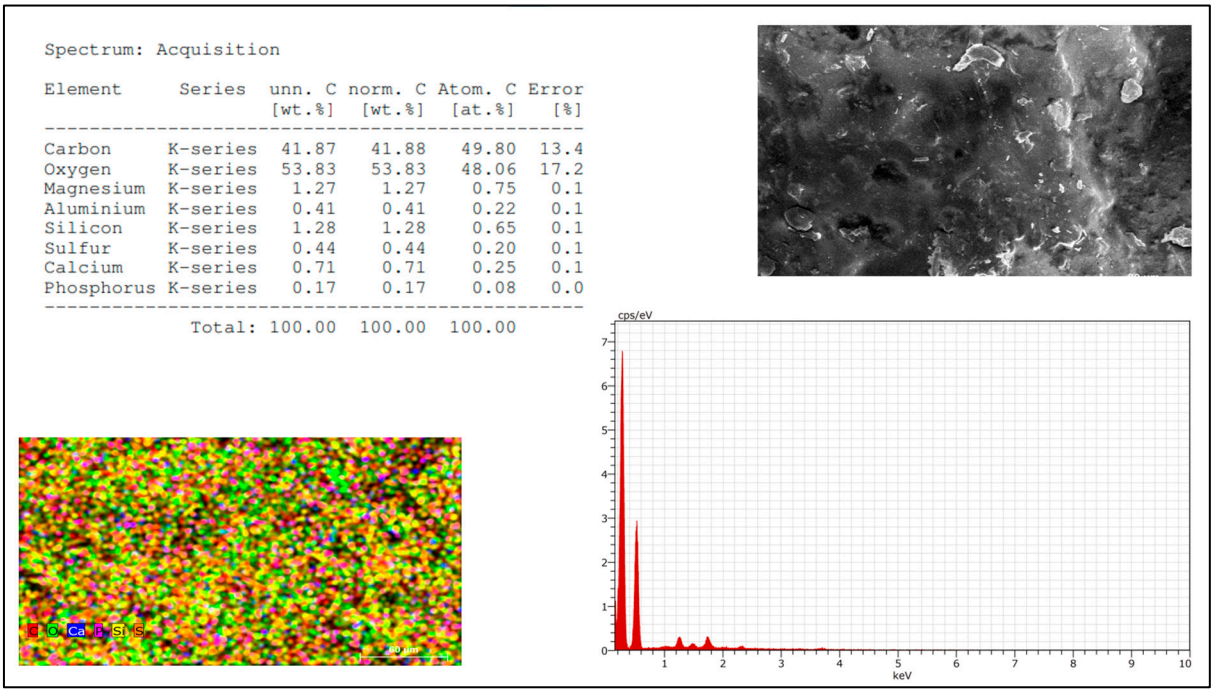

(**b**)

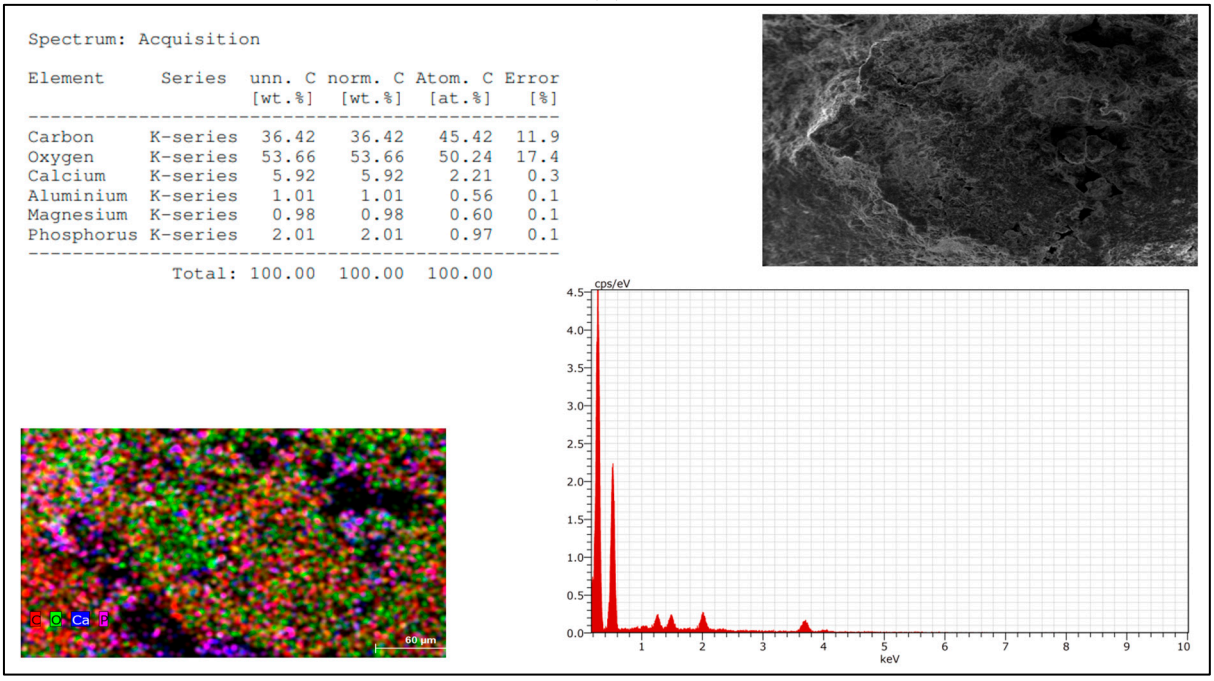

(**c**)

Figure 7. Results of the chemical composition (where, green color marks oxygen, red-carbon, blue-calcium and pink-phosphorus) and morphology of (**a**) sample 1, (**b**) sample 2 and (**c**) sample 3.

Carbon and oxygen suggest the presence of organic substances in printed scaffolds (Figure 7). Thus, PLA was primarily composed of carbon (C) and oxygen (O), with smaller amounts of hydrogen (H). PHA was also composed of carbon (C), oxygen (O) and hydrogen (H). PHB was primarily composed of carbon (C) and hydrogen (H), with oxygen (O). Generally, hydroxyapatite is a calcium phosphate compound and contains calcium (Ca), phosphorus (P), oxygen (O) and magnesium (Mg), which was added separately to the compound. The identified calcium and phosphorus appeared to be connected to hydroxya-

patite, a typical component in bone graft materials. Moreover, organic components such as PLA, PHA or PHB may be responsible for the presence of carbon and oxygen.

3.3. Investigations of the Crystallographic Structure

Investigations of XRD patterns indicated the crystalline properties of composite samples and aided in determining their miscibility and quality, such as crystallinity. This property greatly influences mechanical strength and resorption rate. Understanding these qualities allows creating bone transplant materials that successfully resemble native bone and facilitate tissue regeneration. These findings explained the crystallinity and miscibility of composite materials, the highest intensity peaks and their corresponding diffraction angles. The results (Figure 8) gave the raw and removed Ka2 radiation data in the graph (Figure 8), where the relation between maximum intensity (I) and diffraction angle (2θ) for the three samples was defined. In sample 1, the main peaks were observed at 2θ 16.64° (I = 7846) and 31.74° (I = 9532); sample 2—the main peaks were observed at 2θ 16.70° (I = 11,014) and 31.83° (I = 10,674); sample 3—the main peaks were observed at 2θ 16.56° (I = 7324) and 31.66° (I = 12,525). Removed Ka2 radiation (main peaks) for sample 1 were observed at 2θ 25.80° (I = 2182) and 31.72° (I = 6166); sample 2—observed at 2θ 25.91° (I = 2064) and 31.82° (I = 5536); and sample 3—at 2θ 25.72° (I = 3033) and 31.63° (I = 8564).

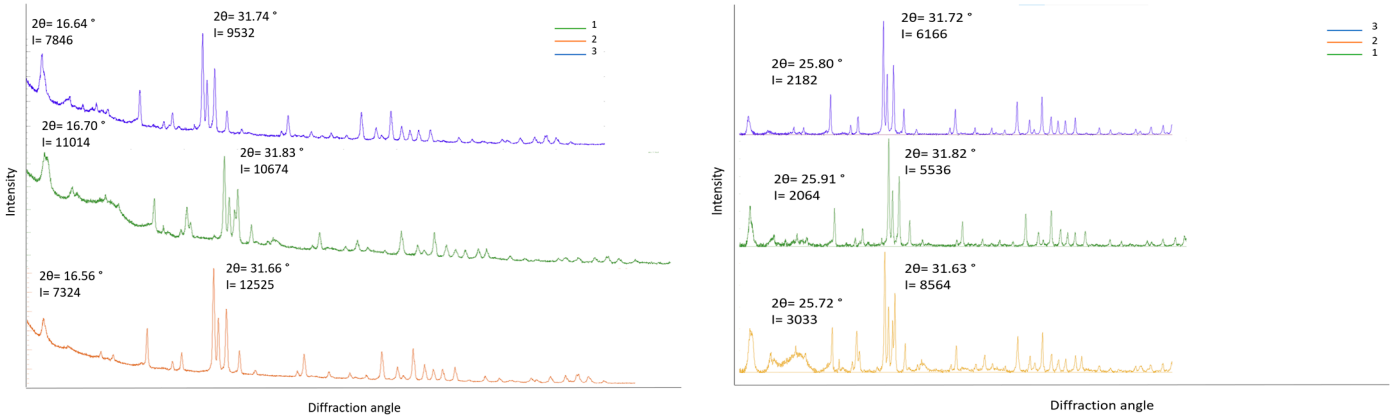

(**a**) (**b**)

Figure 8. (**a**) Raw XRD data from each sample (1, 2 and 3), covering a diffraction angle range of 2 31.66° to 2 31.83°. (**b**) Removed Ka2 radiation data.

Thus, comparing the XRD data of three samples (Figure 8), it appeared that sample 3 had the highest peak intensity at 2 31.66° (I = 12,525), indicating a higher degree of crystallinity or a higher concentration of the crystalline phase in the material. Sample 2 had an intermediate peak intensity at 2 31.83° (I = 10,674). Sample 1 had the lowest peak intensity at 2 31.74° (I = 9532). The higher crystallinity of sample 3 may be implied by a more organised and structured crystal domain layout. Moreover, one of the important factors for biodegradable grafts is the resorption rate of the material. Thus, sample 2 exhibited moderate crystallinity leading to a balance between mechanical strength and resorption rate. Sample 1 demonstrated a decrease in crystallinity or crystalline phase concentration. Results implied suitability of samples for applications where rapid resorption and repair by natural bone tissue is required.

To aid tissue regeneration, the substance used in bone grafting should ideally resemble the qualities of natural bone. Increased crystallinity can occasionally result in increased mechanical strength, which is advantageous for load-bearing bone transplants. Biocompatibility, degradation rate, osteoconductivity and osteoinductivity are all essential considerations in addition to crystallinity requiring rigorous biocompatibility and in vivo studies to evaluate the real performance of these samples in bone transplant applications.

The choice of sample could be determined by the individual clinical scenario and the patient needs to identify which sample would be more preferable for a certain application.

3.4. Investigations of Mechanical Properties

A total of three samples of each compound were tested to evaluate the mechanical strength. The size of the hydroxyapatite (HA) particles, determined by scanning electron microscopy (SEM), ranged from 238 to 757 nm. The mechanical properties were performed with Tinius Olsen H10KT to evaluate the tensile and compressive properties. During the experimentations for more precise data, a total of three test pieces of each sample were taken to evaluate the mechanical strength. Calculations of the tensile strength, compressive yield strength, and Young's modulus for composite materials may give vital insight into how the material will behave under various loading scenarios. For instance, understanding a material's tensile strength can assist in determining how well it can withstand forces such as stretching or tugging, while understanding a material's compressive yield strength can reveal how well it can withstand compression. These characteristics may guarantee the consistency and calibre of composite materials. Thus, the material's capacity to endure pulling or stretching forces was measured by its tensile strength. The investigations evaluated when samples began to fail under compression or when they will be crushed. Young's modulus gauges a material's rigidity or stiffness, helping to understand how much a material will deform in response to a specific load. This is essential to anticipating structural deflections and to ensuring that they stay within allowable limits (Table 3).

Table 3. Properties of materials for sample preparation.

Sample	Force at Break (N)	Displacement at Maximum Force (ΔL)	Elongation at Break (ε_Break)	Tensile Strength, (σ_t)	Young's Modulus (E)	Cross-Sectional Area (A)
1	4365 N	10.45%	14%	12.59 MPa	119.31 MPa	346.36 mm^2
2	1416 N	10.51%	16.75%	4.09 MPa	39.75 MPa	346.36 mm^2
3	1328 N	11.85%	13.733%	39.75 MPa	31.86 MPa	346.36 mm^2

Obtained results showed (Table 3) that sample 3 had a significantly higher tensile strength (39.75 MPa) and sample 2 had the lowest tensile strength (4.09 MPa). Sample 1 had the highest Young's modulus (119.31 MPa), indicating that it is relatively stiff and less deformable under load. Sample 3 had the lowest Young's modulus (31.86 MPa), suggesting that it is relatively flexible and deformable under load. The strongest and stiffest of the three samples—sample 1—had the highest tensile strength and Young's modulus. Sample 3 was strong but comparatively more flexible, since it had a high tensile strength but a lower Young's modulus. The weakest and most stiff of the three samples was sample 2; i.e., it had the lowest tensile strength and a moderate Young's modulus. The stress–strain curve under tensile load illustrated the relationship between stress and strain for each sample. Sample 1 demonstrated the highest tensile strength (12.59 MPa) and Young's modulus (119.31 MPa), indicating superior stiffness and resistance to deformation. In contrast, Sample 2 exhibited the lowest tensile strength (4.09 MPa) with a moderate Young modulus (39.75 MPa), while Sample 3 displayed intermediate properties. Moreover, Sample 3 demonstrated the highest compressive yield strength (39.75 MPa), implying robust resistance to compression. Although sample 1 exhibited a lower compressive yield strength compared to Sample 3, it still showed considerable strength. However, sample 2 exhibited the lowest compressive strength among the samples (Figure 9).

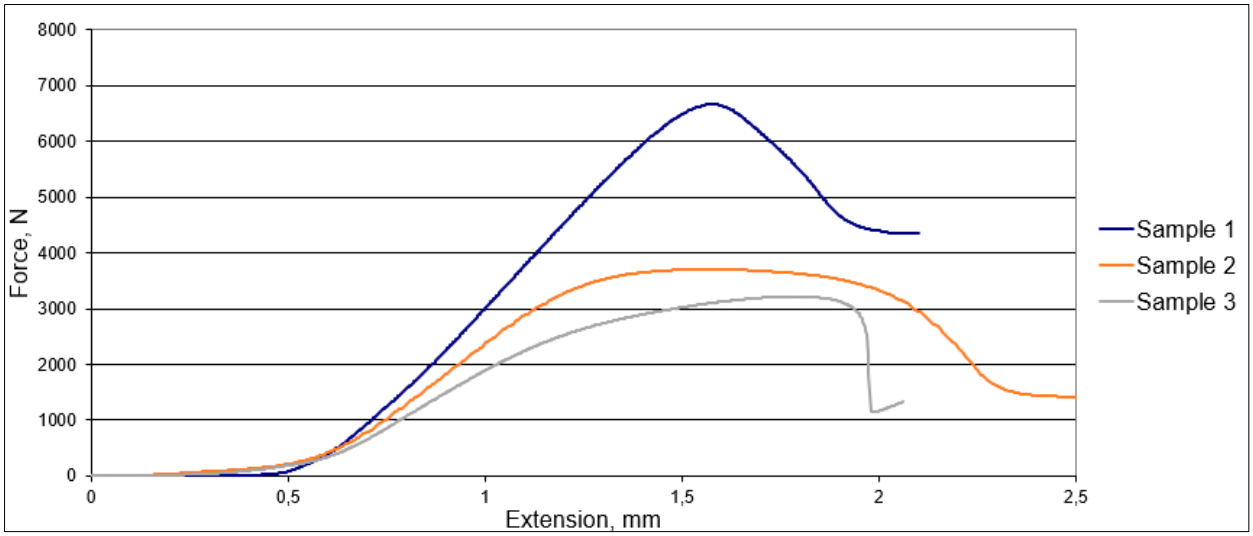

Figure 9. Force–extension curves that depict the mechanical behaviour of composite materials under tension and compression.

These curves offer valuable information on the mechanical behaviour of the composite materials, contributing to their characterisation and enhancing understanding of their performance under diverse loading conditions.

After tensile test measurements, using SEM, 3D images were taken to better understand the structure and porosity (Figure 10).

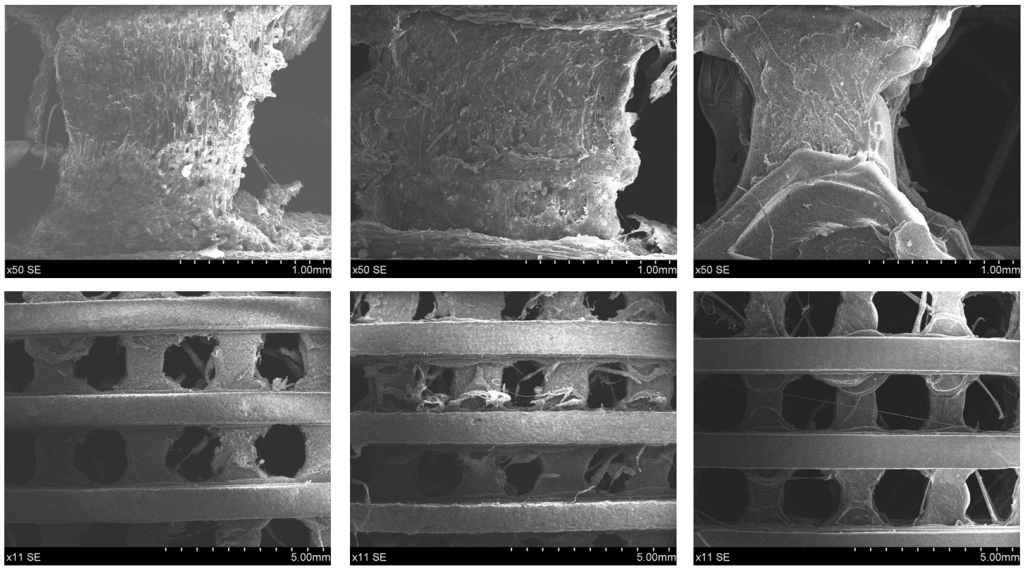

(**a**) (**b**) (**c**)

Figure 10. Three-dimensional image of the structure after the pressure test of (**a**) sample 1, (**b**) sample 2 and (**c**) sample 3.

Hence, the SEM results (Figure 10) showed that the samples under pressure had good porosity with a pore size of 0.8 mm in each sample and the structure itself did not change after the print; however, sum fractures appeared inside the pores of the samples (Figure 11).

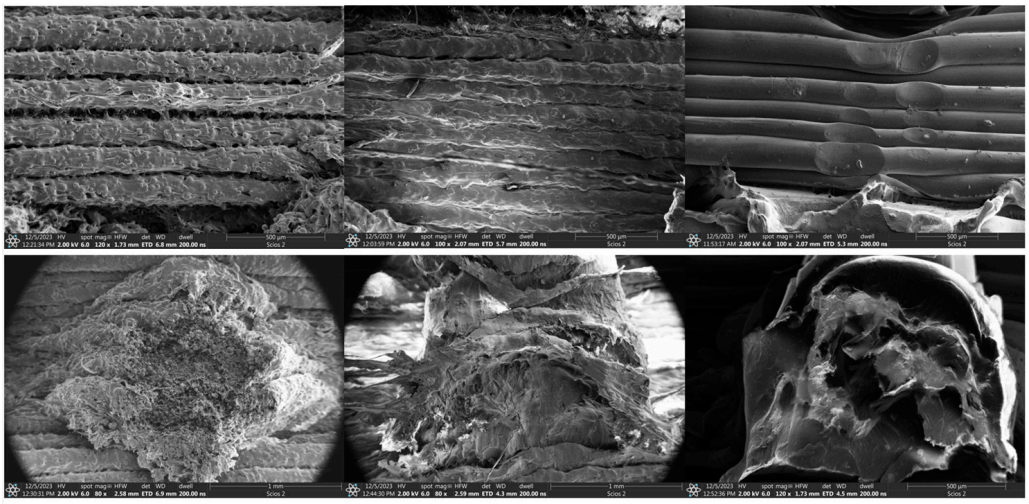

(**a**) (**b**) (**c**)

Figure 11. Three-dimensional fracture images after pressure was applied for (**a**) sample 1, (**b**) sample 2 and (**c**) sample 3.

Porosity is critical in bone grafting, because it directly affects the graft material. Implant porosity affects its potential to stimulate bone growth and vascularisation, which are required for successful integration with recipient bone tissue. A high porosity level promotes nutrition diffusion, cell migration and tissue regeneration. Too little porosity can impede cell infiltration and limit bone development, while too much porosity may affect structural integrity. Furthermore, the weight-to-volume ratio of the composites used in the printed scaffolds was 1.417 g/cm^3. For evaluation of the samples' porosity, the following formula was used:

$$porosity = \frac{\text{Volume of pore space}}{\text{Total volume}} \times 100\% \quad (1)$$

For sample 2:

$$p = \frac{37662340307.63\ \mu m^3}{553616086686.88\ \mu m^3} = 6.80\% \quad (2)$$

For sample 3:

$$p = \frac{33988399576.15\ \mu m^3}{544246204253.61\ \mu m^3} = 6.25\% \quad (3)$$

4. Discussion

Living bone is a dynamic, vascularised tissue made up of mineral, collagen (type I), water and small amounts of other organic substances such as polysaccharides, proteins, proteoglycans, sialoproteins and lipids [15–17]. The ideal scaffold for filling a bone defect should meet the certain requirements. To support bone growth, the scaffold must, first, have a sufficient elastic modulus and compressive strength. Additionally, because natural bone is made up of both organic and inorganic components (calcium phosphate), the right concentration of calcium phosphate ions can stimulate bone growth, and implants must have biological activity. The third requirement is that the scaffold have a 3D pore structure, which is an essential part of the 3D structure. Finally, the scaffold should gradually deteriorate as the new bone grows [18,19]. The main bone mineral, hydroxyapatite (HA), oversees the necessary structural support. The cellular phase of bone is also composed of four main cell types: osteoblasts, which form bone tissue, osteoclasts, which resorb bone tissue, osteocytes, which maintain bone tissue, and bone lining cells [20]. In this study, to meet the mechanical and degradation requirements of load-bearing bone scaffolds, polymer materials were selected as the main part of the scaffolds [21].

The effects of many polymers, such as PHA, PLA and PHB, on bone defect repair were compared. The choice of polymer materials as the main components of bone scaffolds was the subject of this study. Due to their adaptability and customisable qualities, polymers have become increasingly popular in the field of tissue engineering [22]. Notably, biodegradable polymers have gained popularity as promising material for bone scaffolds that bear weight due to their ability to balance mechanical integrity and degradation profiles. In the investigation, various biodegradable polymers were meticulously compared, with a focus on polyhydroxyalkanoates (PHA), polylactic acid (PLA) and poly(3-hydroxybutyrate) (PHB). Each of these polymers has unique qualities that might help repair bone defects. However, selecting one over the other requires careful consideration of mechanical strength, degradation kinetics and biocompatibility [23]. As the primary inorganic component of human bones, HA is stable, biocompatible and easily degraded. These properties help to promote osteoblast adhesion and proliferation, as well as extracellular matrix and the formation of chemical bonds with natural bone [24,25].

5. Conclusions

The selection of composite materials is crucial in tissue engineering because it directly affects the biocompatibility and the properties of the scaffold. In this study, different weight percentages of polylactic acid (PLA), polyhydroxyalkanoate (PHA), poly(3-hydroxybutyrate) and hydroxyapatite (HA) were combined. These substances were chosen because they are promising candidates for tissue-engineering applications and are biocompatible and biodegradable. SEM analysis confirmed the favourable dispersion of HA and compatibility within the PHB/PHA/PLA matrix, raising the possibility of increased bioactivity and osteoconductivity. HA is a valuable addition to tissue-engineered scaffolds due to its excellent biocompatibility and capacity to support bone regeneration.

The elemental composition was confirmed by EDS, the surface shape and microstructure were revealed by SEM, and the crystalline structure and phase composition were evaluated by XRD. SEM analysis showed visual proof of the composite's structural traits, particle distribution, interface compatibility, porous structure and uniform distribution of hydroxyapatite particles throughout the scaffold matrix. The potential to mimic the mineral makeup of natural bone is indicated by the proper dispersion of HA within them. The samples were printed with a 3D printer, keeping the pore size at 0.8 mm in each sample.

The results of mechanical tests, which consider factors like tensile and compressive strength, were crucial in determining how well the scaffolds can withstand physiological forces. To ensure that they can maintain their structural integrity during the dynamic process of tissue regeneration, it was essential to understand their mechanical behaviour. The investigations showed that the best results were obtained for sample 2, which had a higher porosity level compared to the others, which promotes better diffusion of nutrition, cell migration and tissue regeneration. The strongest and stiffest of the three samples was sample 1 with the highest tensile strength and Young's modulus; sample 3 was strong, but comparatively more flexible, and the weakest and most stiff of the three samples was sample 2—it had the lowest tensile strength and a moderate Young's modulus.

The designed scaffolds underwent a thorough evaluation process to ensure that they were not only strong and stable but also had the potential to make a significant contribution to the study of tissue regeneration and repair. When it comes to the functionality and stability of tissue-engineered scaffolds, mechanical properties are extremely important.

Author Contributions: Conceptualisation, M.S.R. and G.J.; methodology, M.S.R., A.P. and D.P.; validation, M.S.R., G.J. and S.U.; formal analysis, A.P. and D.P.; investigation, M.S.R., D.P. and S.U.; writing—original draught preparation, M.S.R.; writing—review and editing, S.U. and G.J. All authors have read and agreed to the published version of the manuscript.

Funding: This research received no external funding.

Data Availability Statement: Data are contained within the article.

Conflicts of Interest: The authors declare no conflicts of interest.

References

1. Mirkhalaf, M.; Men, Y.; Wang, R.; No, Y.; Zreiqat, H. Personalized 3D printed bone scaffolds: A review. *Acta Biomater.* **2023**, *156*, 110–124. [CrossRef] [PubMed]
2. Rengier, F.; Mehndiratta, A.; von Tengg-Kobligk, H.; Zechmann, C.M.; Unterhinninghofen, R.; Kauczor, H.U.; Giesel, F.L. 3D printing based on imaging data: Review of medical applications. *Int. J. CARS* **2010**, *5*, 335–341. [CrossRef] [PubMed]
3. Bose, S.; Vahabzadeh, S.; Bandyopadhyay, A. Bone tissue engineering using 3D printing. *Mater. Today* **2013**, *16*, 496–504. [CrossRef]
4. Hutmacher, D.W. Scaffolds in tissue engineering bone and cartilage. *Biomaterials* **2000**, *21*, 2529–2543. [CrossRef] [PubMed]
5. Ogueri, K.S.; Jafari, T.; Escobar Ivirico, J.L. Laurencin Polymeric Biomaterials for scaffold-based bone regenerative engineering. *Regen. Eng. Transl. Med.* **2019**, *5*, 128–154. [CrossRef] [PubMed]
6. Chiara, G.; Letizia, F.; Lorenzo, F.; Edoardo, S.; Diego, S.; Stefano, S.; Eriberto, B.; Barbara, Z. Nanostructured biomaterials for tissue engineered bone tissue reconstruction. *Int. J. Mol. Sci.* **2012**, *13*, 737–757. [CrossRef] [PubMed]
7. Carluccio, D.; Xu, C.; Venezuela, J.; Cao, Y.; Kent, D.; Bermingham, M.; Demir, A.G.; Previtali, B.; Ye, Q.; Dargusch, M. Additively manufactured iron-manganese for biodegradable porous load-bearing bone scaffold applications. *Acta Biomater.* **2020**, *103*, 346–360. [CrossRef] [PubMed]
8. Cockerill, I.; Su, Y.; Sinha, S.; Qin, Y.X.; Zheng, Y.; Young, M.L.; Zhu, D. Porous zinc scaffolds for bone tissue engineering applications: A novel additive manufacturing and casting approach. *Mater. Sci. Eng. C* **2020**, *110*, 110738. [CrossRef] [PubMed]
9. Mangano, F.; Macchi, A.; Shibli, J.A.; Luongo, G.; Iezzi, G.; Piattelli, A.; Caprioglio, A.; Mangano, C. Maxillary ridge augmentation with custom-made CAD/CAM scaffolds. A1-year prospective study on 10 patients. *J. Oral Implantol.* **2014**, *40*, 561–569. [CrossRef]
10. Azad, M.A.; Olawuni, D.; Kimbell, G.; Badruddoza, A.Z.M.; Hossain, M.S.; Sultana, T. Polymers for Extrusion-Based 3D Printing of Pharmaceuticals: A Holistic Materials–Process Perspective. *Pharmaceutics* **2020**, *12*, 124. [CrossRef]
11. Iqbal, N.; Khan, A.S.; Asif, A.; Yar, M.; Haycock, J.W. Recent concepts in biodegradable polymers for tissue engineering paradigms: A critical review. *Int. Mater. Rev.* **2018**, *64*, 91–126. [CrossRef]
12. Brunello, G.; Sivolella, S.; Meneghello, R.; Ferroni, L.; Gardin, C.; Piattelli, A.; Zavan, B.; Bressan, E. Powder-based 3D printing for bone tissue engineering. *Biotechnol. Adv.* **2016**, *34*, 740–753. [CrossRef] [PubMed]
13. Li, Q.; Ma, L.; Gao, C. Biomaterials for in situ tissue regeneration: Development and perspectives. *J. Mater. Chem. B* **2015**, *3*, 8921–8938. [CrossRef] [PubMed]
14. Xie, Z.; Gao, M.; Lobo, A.O.; Webster, T.J. 3D Bioprinting in Tissue Engineering for Medical Applications: The Classic and the Hybrid. *Polymers* **2020**, *12*, 1717. [CrossRef] [PubMed]
15. Deng, C.; Lin, R.; Zhang, M.; Qin, C.; Yao, Q.; Wang, L.; Chang, J.; Wu, C. Micro/nanometer-structured scaffolds for regeneration of both cartilage and subchondral bone. *Adv. Funct. Mater.* **2019**, *29*, 1806068. [CrossRef]
16. Lee, S.Y. Bacterial polyhydroxyalkanoates. *Biotechnol. Bioeng.* **1996**, *49*, 1–14. [CrossRef]
17. Yousefiasl, S.; Sharifi, E.; Salahinejad, E.; Makvandi, P.; Irani, S. Bioactive 3D-printed chitosan-based scaffolds for personalized craniofacial bone tissue engineering. *Eng. Regen.* **2023**, *4*, 1–11. [CrossRef]
18. Huang, J.; Xia, X.; Zou, Q.; Ma, J.; Jin, S.; Li, J.; Zuo, Y.; Li, Y. The long-term behaviors and differences in bone reconstruction of three polymer-based scaffolds with different degradability. *J. Mater. Chem. B* **2019**, *7*, 7690–7703. [CrossRef] [PubMed]
19. Wang, J.L.; Xu, J.K.; Hopkins, C.; Chow, D.H.; Qin, L. Biodegradable Magnesium-Based Implants in Orthopedics—A General Review and Perspectives. *Adv. Sci.* **2020**, *7*, 1902443. [CrossRef]
20. Amna, T. Valorization of Bone Waste of Saudi Arabia by Synthesizing Hydroxyapatite. *Appl. Biochem. Biotechnol.* **2018**, *186*, 779–788. [CrossRef]
21. Yazdanpanah, Z.; Bahrololoom, M.E.; Hashemi, B. Evaluating morphology and mechanical properties of glass-reinforced natural hydroxyapatite composites. *J. Mech. Behav. Biomed. Mater.* **2015**, *41*, 36–42. [CrossRef] [PubMed]
22. Zarei, M.; Shabani Dargah, M.; Hasanzadeh Azar, M.; Alizadeh, R.; Mahdavi, F.S.; Sayedain, S.S.; Kaviani, A.; Asadollahi, M.; Azami, M.; Beheshtizadeh, N. Enhanced bone tissue regeneration using a 3D-printed poly(lactic acid)/Ti6Al4V composite scaffold with plasma treatment modification. *Sci. Rep.* **2023**, *13*, 3139. [CrossRef] [PubMed]
23. Florencio-Silva, R.; Sasso, G.R.; Sasso-Cerri, E.; Simões, M.J.; Cerri, P.S. Biology of Bone Tissue: Structure, Function, and Factors That Influence Bone Cells. *BioMed Res. Int.* **2015**, *2015*, 421746. [CrossRef] [PubMed]
24. Angili, S.N.; Morovvati, M.R.; Kardan-Halvaei, M.; Saber-Samandari, S.; Razmjooee, K.; Abed, A.M.; Toghraie, D.; Khandan, A. Fabrication and finite element simulation of antibacterial 3D printed Poly L-lactic acid scaffolds coated with alginate/magnesium oxide for bone tissue regeneration. *Int. J. Biol. Macromol.* **2023**, *224*, 1152–1165. [CrossRef]
25. Seoane-Viaño, I.; Trenfield, S.J.; Basit, A.W.; Goyanes, A. Translating 3D printed pharmaceuticals: From hype to real-world clinical applications. *Adv. Drug Deliv. Rev.* **2021**, *174*, 553–575. [CrossRef]